HAL
open science

Graph-Cut-Based Model for Spectral-Spatial Classification of Hyperspectral Images

Yuliya Tarabalka, Aakanksha A Rana

To cite this version:

Yuliya Tarabalka, Aakanksha A Rana. Graph-Cut-Based Model for Spectral-Spatial Classification of Hyperspectral Images. IEEE IGARSS - International Geoscience and Remote Sensing Symposium, Jul 2014, Quebec, Canada. hal-01011495

HAL Id: hal-01011495

https://inria.hal.science/hal-01011495v1

Submitted on 24 Jun 2014

HAL is a multi-disciplinary open access archive for the deposit and dissemination of scientific research documents, whether they are published or not. The documents may come from teaching and research institutions in France or abroad, or from public or private research centers.

L'archive ouverte pluridisciplinaire **HAL**, est destinée au dépôt et à la diffusion de documents scientifiques de niveau recherche, publiés ou non, émanant des établissements d'enseignement et de recherche français ou étrangers, des laboratoires publics ou privés.

GRAPH-CUT-BASED MODEL FOR SPECTRAL-SPATIAL CLASSIFICATION OF HYPERSPECTRAL IMAGES

Yuliya Tarabalka and Aakanksha Rana

Inria Sophia-Antipolis Méditerranée, AYIN team,
2004 route des Lucioles, 06902 Sophia Antipolis, France
e-mail: yuliya.tarabalka@inria.fr

ABSTRACT

We propose a new spectral-spatial method for hyperspectral image classification based on a graph cut. The classification task is formulated as an energy minimization problem on the graph of image pixels, and is solved by using the graph-cut α-expansion approach. The energy to optimize is computed as a sum of data and interaction energy terms, respectively. The data energy term is computed using the outputs of the probabilistic support vector machines classification. The second energy term, which expresses the interaction between spatially adjacent pixels, is computed by using dissimilarity measures between spectral vectors, such as vector norms, spectral angle mapper and spectral information divergence. Experimental results on hyperspectral images captured by the ROSIS and the AVIRIS sensors reveal that the proposed method yields higher classification accuracies when compared to the recent state-of-the-art approaches.

***Index Terms*—** Hyperspectral images, graph cut, multi-label alpha expansion, contextual information, support vector machines.

1. INTRODUCTION

The very high spectral and spatial resolution of the latest generation of remote sensors provides rich information for every pixel in an image scene, hence opening new perspectives in classification, but also presenting challenges of high-volume data analysis. The recent overview of hyperspectral image classification methods points out the importance of exploiting both spatial and spectral information in a classifier [1].

Markov random fields (MRFs) are probabilistic models that are widely used to include spatial context into image-analysis schemes in terms of minimization of suitable energy functions [2]. While earlier algorithms for optimizing MRF energy, such as iterated conditional modes (ICM) and simulated annealing [3, 4] were time consuming, more advanced methods, such as graph cuts [5] provided powerful alternatives from both theoretical and computational viewpoints, resulting in a growing use of the MRF-based techniques.

The commonly used MRF energy function for image classification is computed as a linear combination of two terms: 1) The first term E_{data} is related to pixelwise information and it measures for each pixel the disagreement between a prior probabilistic model and the observed data. 2) The second contribution E_{smooth} expresses interaction between neighboring pixels, thus exploiting image spatial context. Most works in remote sensing image classification use a Potts model [2, 6] to compute this spatial term, which favors spatially adjacent pixels to belong to the same class. The drawback of the Potts model is that it tends to penalize the classification accuracy around the edges between different classes. To mitigate this drawback, "edge-preserving" functions have been proposed and integrated in the MRF energy function [3, 4].

In this work, we propose to formulate the spatial energy term as a function of dissimilarity between spectral vectors of neighboring pixels. We investigate the use of different spectral dissimilarity measures for this purpose, such as vector norms, spectral angle mapper (SAM) and spectral information divergence (SID) [7]. Thus, a new MRF-based method (*SVM-GC*) for hyperspectral image classification is proposed in this paper (Section 2). The spectral energy is computed from the outputs of the probabilistic support vector machines (SVM) classification. The spatial energy is computed by measuring dissimilarity between spectra of adjacent pixels. The resulting MRF energy is optimized by using the graph-cut α-expansion algorithm [5], yielding a spectral-spatial classification map. We validate the performance of the proposed method for classification of two hyperspectral images collected by the Reflective Optics System Imaging Spectrometer (ROSIS) and the Airborne Visible/Infrared Imaging Spectrometer (AVIRIS), respectively (Section 3).

2. PROPOSED METHOD

An input B-band hyperspectral image can be represented as a set of n pixel vectors $\mathbf{X} = \{\mathbf{x}_i \in \mathbb{R}^B, i = 1, 2, ..., n\}$. The goal is to compute a classification map $L = \{L_i, i = 1, 2, ..., n\}$, where each pixel $\mathbf{x}_i$ is assigned to one of K information classes $\{\omega_1, \omega_2, ..., \omega_K\}$, i.e., has a class label L_i.

The proposed *SVM-GC* method comprises two main phases (see Fig. 1):

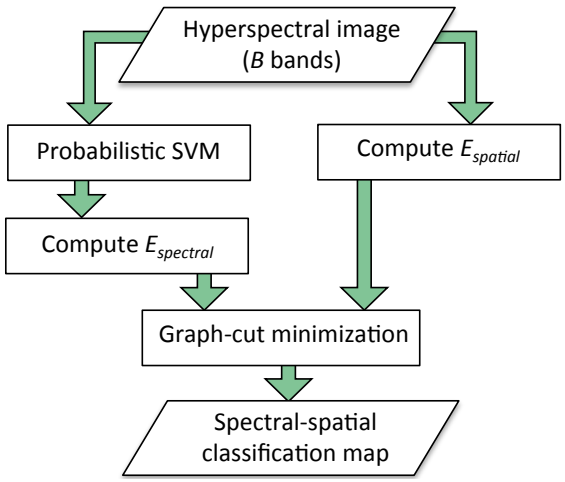

Fig. 1. Flowchart of the proposed *SVM-GC* classification method.

2.1. Probabilistic pixelwise classification

The first phase consists in estimating class probabilities for each pixel $\{p(L_i = k|\mathbf{x}_i), k = 1, ..., K\}, i = 1, 2, ..., n$. We propose to use a probabilistic SVM classifier, which performs well and has been widely applied to analyze hyperspectral data [4, 6, 7]. We refer the reader to [7] for details about estimation of class probabilities by pairwise coupling of binary probability estimates.

2.2. Graph-cut energy minimization

In this phase, the spectral-spatial classification map is computed by minimizing an energy of the form:

$$E(L) \;=\; E_{data}+E_{smooth} = \sum_{i=1}^{n} V_i(L_i) + \sum_{i\sim j} W_{i,j}(L_i, L_j), \tag{1}$$

where individual potentials $V_i(L_i)$ measure a penalty for a pixel i to have a label L_i, $i \sim j$ denotes a pair of spatially adjacent pixels (eight-neighborhood is used in our work), and $W_{i,j}(L_i, L_j)$ are interaction terms between neighboring pixels i and j expressing spatial coherency.

The individual potentials are computed by using the estimated class probabilities for each pixel:

$$V_i(L_i) \;=\; -ln(p(L_i|\mathbf{x}_i)). \tag{2}$$

To compute spatial interaction terms, most studies on remote sensing image analysis employ a Potts model [2]:

$$W_{i,j}(L_i, L_j) \;=\; \beta\,(1 - \delta(L_i, L_j)), \tag{3}$$

where $\delta(\cdot)$ is the Kronecker function ($\delta(a, b) = 1$ for $a = b$ and $\delta(a, b) = 0$ otherwise) and β is a positive constant parameter that controls the importance of spatial smoothing. This model tends to deteriorate classification results at the edges between land-cover classes and near small-scale details. In order to preserve the borders in the classification map, "edge" functions have been proposed and integrated in the spatial energy term, such as [4]:

$$W_{i,j}(L_i, L_j) \;=\; \beta\,(1 - \delta(L_i, L_j))\,\frac{t}{t + |\rho_{i|j}|}, \tag{4}$$

where $\rho_{i|j}$ is the gradient value of the pixel i in the direction of j, and t is a parameter controlling the fuzzy edge threshold.

In this paper, we further investigate how to correctly incorporate the information associated with class edges within the MRF framework. We express the spatial interaction term as a function of dissimilarity between spectra of the adjacent pixels:

$$W_{i,j}(L_i, L_j) \;=\; \beta\,(1 - \delta(L_i, L_j))\,\exp\left[-d(\mathbf{x}_i, \mathbf{x}_j)\right], \tag{5}$$

where $d(\mathbf{x}_i, \mathbf{x}_j)$ measures the discrepancy between the pixel vectors $\mathbf{x}_i = (x_{i1}, ..., x_{iB})^T$ and $\mathbf{x}_j = (x_{j1}, ..., x_{jB})^T$. We explored the use of three dissimilarity measures [7]:

1. $L2$-norm based:

$$d_{L2}(\mathbf{x_i}, \mathbf{x_j}) = \left(\sum_{b=1}^{B} |x_{ib} - x_{jb}|^2|\right) /2\sigma^2\, B, \tag{6}$$

   where σ is a standard deviation of the image spectral values.

2. The SAM distance computes the angle between spectral vectors:

$$d_{SAM}(\mathbf{x}_i, \mathbf{x}_j) = \arccos\left(\frac{\sum\limits_{b=1}^{B} x_{ib}x_{jb}}{\left[\sum\limits_{b=1}^{B} x_{ib}^2\right]^{1/2}\left[\sum\limits_{b=1}^{B} x_{jb}^2\right]^{1/2}}\right). \tag{7}$$

3. The SID-based measure computes the discrepancy of probabilistic behaviors between the spectral signatures of two pixels:

$$d_{SID}(\mathbf{x}_i, \mathbf{x}_j) = \frac{1}{B}\sum_{b=1}^{B}\left(q_b(\mathbf{x}_i)log\left[\frac{q_b(\mathbf{x}_i)}{q_b(\mathbf{x}_j)}\right] + q_b(\mathbf{x}_j)log\left[\frac{q_b(\mathbf{x}_j)}{q_b(\mathbf{x}_i)}\right]\right), \tag{8}$$

   where

$$q_b(\mathbf{x}_i) = \frac{x_{ib}}{\sum_{l=1}^{B} x_{il}}.$$

The resulting energy $E(L)$ is minimized by applying the efficient α-expansion graph-cut-based algorithm described in [5].

Table 1. Overall and Average Classification Accuracies in Percentage (mean $\pm$ standard deviation) for the *Pavia University* and the *Salinas* Data Sets. The Highest Accuracies are **Bolded**.

Image	Accuracy (%)	SVM	SVM-MLR -MRF [6]	*SVM-GC* with different E_{smooth} (the number of Eq. is given in parentheses)				
				$Potts$ (3)	$Edge$ (4)	$L2$ (5, 6)	SAM (5, 7)	SID (5, 8)
Pavia University	Overall	84.50 $\pm$1.41	92.64	94.23 $\pm$ 2.10	94.26 $\pm$ 1.95	95.36 $\pm$ 0.98	96.73 $\pm$ 0.79	**97.26** $\pm$ 0.31
	Average	88.70 $\pm$0.48	90.67	96.11 $\pm$ 0.56	96.13 $\pm$ 0.87	96.44 $\pm$ 1.51	96.96 $\pm$ 0.47	**97.40** $\pm$ 0.28
Salinas	Overall	90.56 $\pm$1.32	-	93.88 $\pm$0.83	93.98 $\pm$1.27	95.70 $\pm$ 1.19	95.20 $\pm$ 1.77	**95.99** $\pm$1.53
	Average	92.56 $\pm$0.47	-	96.92 $\pm$ 0.20	97.07 $\pm$0.56	97.87 $\pm$ 0.46	97.27 $\pm$ 0.92	**98.01** $\pm$0.87

3. EXPERIMENTAL RESULTS AND DISCUSSION

We used two hyperspectral airborne images to evaluate the proposed *SVM-GC* method:

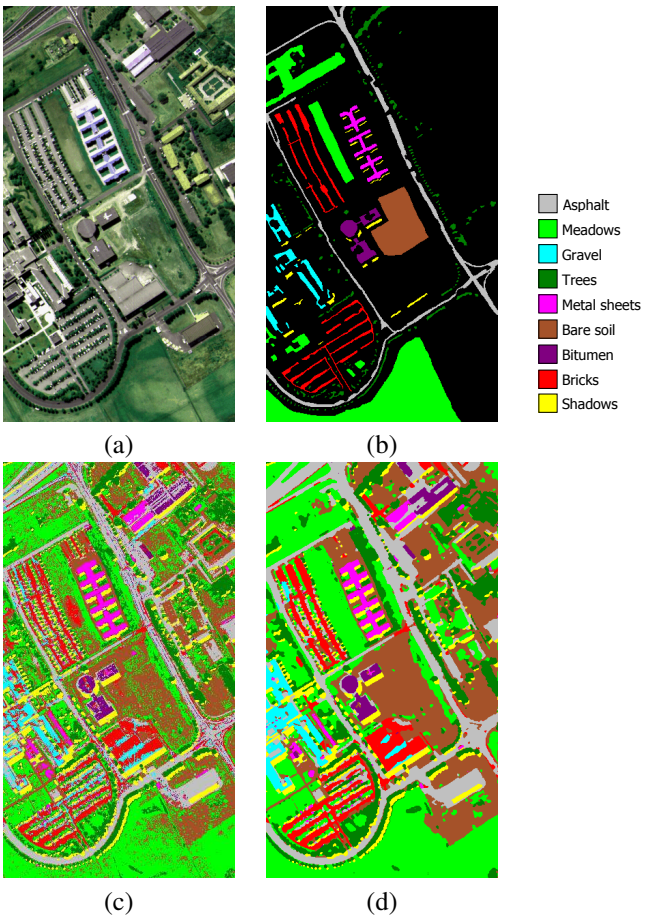

Fig. 2. *Pavia University* image. (a) Three-band color composite. (b) Reference data. (c) SVM classification map. (d) *SVM-GC* classification map when using the SID-based spatial interaction terms.

1. The *Pavia University* image was acquired by the ROSIS sensor over the urban area. It is of 610 by 340 pixels, with a very-high spatial resolution of 1.3 m/pixel and 103 spectral channels. Nine information classes are considered. Fig. 2 shows a three-band false color image and the reference data, which contain 42776 labeled pixels.

2. The *Salinas* image was recorded by the AVIRIS sensor over the agricultural area. The covered area comprises 512 lines by 217 samples, with a spatial resolution of 3.7 m/pixel and 224 spectral bands. The reference data contain sixteen thematic classes and 50550 labeled pixels.

More information about both images, with the number of labeled samples per class, can be found in [8]. Fifty samples for each class were randomly selected from the reference data as training samples. The remaining samples composed the test set.

In all experiments, the probabilistic one *versus* one SVM classification with the Gaussian radial basis function (RBF) was performed. The optimal values for the parameters C (parameter that controls the amount of penalty during the SVM optimization) and γ (spread of the RBF kernel) were tuned by fivefold cross validation from the range of $[2^{-5}, 2^{15}]$ and $[2^{-15}, 2^{5}]$, respectively. Then, the α-expansion graph-cut-based optimization on the image graph was applied, using different interaction terms described in Section 2. For this purpose, the individual potentials were determined by Eq. (2), and the interaction terms were computed by using one of Equations (3-5), where in Eq. 5 we compared the use of three dissimilarity measures given by Equations (6-8). The optimal value of the parameter $\beta = 0.75$ was experimentally derived. Alternatively, this MRF smoothing parameter can be automatically estimated by using the state-of-the-art techniques, such as [9, 10]. The parameter t was tuned by following the recommendations from [4].

Table 1 summarizes the global (overall and class-average) classification accuracies for both data sets, for the SVM and the proposed *SVM-GC* methods. We ran each classification experiment five times, each time with different training-test set, with the randomly chosen fifty training samples per class. The mean accuracies and the standard deviations are reported in the table. We included for comparison the results from the recently published work [6] on MRF-based hyperspectral image classification (SVM-MLR-MRF), where the data energy term is computed by combining probabilistic SVM and subspace-based multinomial logistic regression, and the spa-

tial information is exploited by means of the Potts model. The authors also classified the *Pavia University* image and used fifty randomly selected samples per class for training, hence these results are comparable to ours.

As can be seen from the table, the obtained results are coherent for both images. The graph-cut-based *SVM-GC* method with the simple Potts model (3) yields significantly higher classification accuracies when compared to the SVM results. For the *Pavia University* image, the overall and the average accuracies are improved by 9.73 and by 7.41 percentage points, respectively. By comparing the results with those obtained with the stochastic Metropolis algorithm to optimize the MRF energy [4], one can conclude that the graph-cut-based optimization yields higher classification accuracies in a lower computational time. The *SVM-GC* accuracies are also higher when compared to the SVM-MLR-MRF results reported in [6]. The integration of the "edge-preserving" function (4) in the spatial energy term does not increase significantly the classification accuracies.

When the proposed formulation of the spatial interaction terms (5) is used, the obtained accuracies are significantly higher than the results obtained with the standard Potts model. The statistically significant difference is validated by the McNemar's test with 5% level of significance. For both images, the use of the *SID*-based spatial interaction term yields the highest classification accuracies. When compared to the Potts model results, the overall accuracy in this case is improved by 3.03 and 2.11 percentage points for the *Pavia University* and the *Salinas* images, respectively. Fig. 2(c-d) compare the corresponding *SVM-GC* classification map for the *Pavia University* image with the SVM classification map. It can be seen from the image that the *SVM-GC* method yields the classification map with homogeneous regions, while preserving the region edges.

4. CONCLUSIONS

In this work, we addressed the problem of spectral-spatial classification of hyperspectral images with very high spatial resolution. We presented a new MRF-based method to solve the classification problem. First, the data energy term is computed from the outputs of the probabilistic SVM classification. Then, we proposed to compute the spatial energy term as a function of dissimilarity between spectral vectors of neighboring pixels. We investigated the use of three dissimilarity criteria for this purpose, namely $L2$ vector norm, SAM and SID measures. The resulting energy is minimized by means of the α-expansion graph-cut-based algorithm. The experimental results on two hyperspectral airborne images did show that the proposed graph-cut-based method outperformed the recent state-of-the-art approaches both in terms of classification accuracies and computational time.

5. REFERENCES

[1] G. Camps-Valls, D. Tuia, L. Bruzzone, and J. A. Benediktsson, "Advances in hyperspectral image classification: Earth monitoring with statistical learning methods," *IEEE Sign. Proc. Magaz.*, vol. 31, no. 1, pp. 45–54, 2014.

[2] G. Moser, S. B. Serpico, and J. A. Benediktsson, "Land-cover mapping by Markov modeling of spatial-contextual information in very-high-resolution remote sensing images," *Proc. of IEEE*, vol. 101, no. 3, pp. 631–651, 2013.

[3] G. Moser and S. B. Serpico, "Combining support vector machines and Markov random fields in an integrated framework for contextual image classification," *IEEE TGRS*, vol. 51, no. 5, pp. 2734–2752, 2013.

[4] Y. Tarabalka, M. Fauvel, J. Chanussot, and J. A. Benediktsson, "SVM- and MRF-based method for accurate classification of hyperspectral images," *IEEE GRSL*, vol. 7, no. 4, pp. 736–740, 2010.

[5] Y. Boykov, O. Veksler, and R. Zabih, "Fast approximate energy minimization via graph cuts," *IEEE TPAMI*, vol. 23, no. 11, pp. 1222–1239, 2001.

[6] M. Khodadadzadeh, J. Li, A. Plaza, H. Ghassemian, and J. M. Bioucas-Dias, "Spectral-spatial classification for hyperspectral data using SVM and subspace MLR," in *Proc. of IGARSS'13*, Melbourne, Australia, 2013.

[7] Y. Tarabalka, J. Chanussot, and J. A. Benediktsson, "Segmentation and classification of hyperspectral images using minimum spanning forest grown from automatically selected markers," *IEEE Trans. Systems, Man, and Cyb.: Part B*, vol. 40, no. 5, pp. 1267–1279, Oct. 2010.

[8] Grupo de Inteligencia Computacional, "Hyperspectral remote sensing scenes," http://www.ehu.es/ccwintco/index.php/Hyperspectral_Remote_Sensing_Scenes, 2012.

[9] S. B. Serpico and G. Moser, "Weight parameter optimization by the Ho-Kashyap algorithm in MRF models for supervised image classification," *IEEE TGRS*, vol. 44, no. 12, pp. 3695–3705, 2006.

[10] H. Aghighi, J. Trinder, Y. Tarabalka, and S. Lin, "Dynamic block-based parameter estimation for MRF classification of high-resolution images," *IEEE GRSL*, vol. PP, no. 99, pp. 1–5, 2014.